SANDIA REPORT

SAND2017-7851
Unlimited Release
Printed July 2017

Radar Doppler Processing with Nonuniform Sampling

Armin W. Doerry

Prepared by
Sandia National Laboratories
Albuquerque, New Mexico 87185 and Livermore, California 94550

Sandia National Laboratories is a multimission laboratory managed and operated by National Technology and Engineering Solutions of Sandia, LLC., a wholly owned subsidiary of Honeywell International, Inc., for the U.S. Department of Energy's National Nuclear Security Administration under contract DE-NA-0003525.

Issued by Sandia National Laboratories, operated for the United States Department of Energy by Sandia Corporation.

Available to DOE and DOE contractors from

U.S. Department of Energy
Office of Scientific and Technical Information
P.O. Box 62
Oak Ridge, TN 37831

Telephone: (865) 576-8401
Facsimile: (865) 576-5728
E-Mail: reports@adonis.osti.gov
Online ordering: http://www.osti.gov/bridge

Available to the public from

U.S. Department of Commerce
National Technical Information Service
5285 Port Royal Rd.
Springfield, VA 22161

Telephone: (800) 553-6847
Facsimile: (703) 605-6900
E-Mail: orders@ntis.fedworld.gov
Online order: http://www.ntis.gov/help/ordermethods.asp?loc=7-4-0#online

SAND2017-7851
Unlimited Release
Printed July 2017

Radar Doppler Processing with Nonuniform Sampling

Armin W. Doerry
ISR Mission Engineering
Sandia National Laboratories
PO Box 5800
Albuquerque, NM 87185-0519

Abstract

Conventional signal processing to estimate radar Doppler frequency often assumes uniform pulse/sample spacing. This is for the convenience of the processing. More recent performance enhancements in processor capability allow optimally processing nonuniform pulse/sample spacing, thereby overcoming some of the baggage that attends uniform sampling, such as Doppler ambiguity and SNR losses due to sidelobe control measures.

Acknowledgements

This report was the result of an unfunded research and development activity.

Contents

Foreword

This report details the results of an academic study. It does not presently exemplify any modes, methodologies, or techniques employed by any operational system known to the author.

Classification

The specific mathematics and algorithms presented herein do not bear any release restrictions or distribution limitations.

This report formalizes preexisting informal notes and other documentation on the subject matter herein.

1 Introduction and Background

The realm of pulse-Doppler radar systems is defined by the action of a sequence of pulses being transmitted, with echoes therefrom recorded and processed. Conventional processing across pulses especially in coherent systems often assumes the pulses are equally spaced, either in time or in spatial offset. We observe that radar modes that attempt to measure velocity, such as Ground Moving Target Indicator (GMTI) radar, typically attempt to collect data with uniform spacing in time. However, radar modes that attempt to measure spatial frequencies, such as Synthetic Aperture Radar (SAR), may be operated to collect data with some degree of uniform spacing in distance (for example slaving sample timing to velocity).

Uniform sample spacing is particularly convenient for conventional processing schemes that often employ efficient transforms such as the Fast Fourier Transform (FFT) for Doppler frequency calculations. Even when the collected data is not precisely uniform, data samples are typically resampled to a uniform spacing for subsequent processing. For data that are uniformly sampled, or even nearly so, a problematic consequence is the manifestation of grating lobes in their spectrum, leading to ambiguous Doppler frequency measures. We emphasize the point that strong Doppler grating lobes are a direct consequence of uniform sample spacing. In addition, another consequence to any Doppler frequency notches, such as for stationary clutter suppression, is that they too are repeated to form periodic "blind" velocities. Furthermore, a Doppler spectral analysis of uniform samples often requires amplitude tapering to control deleterious sidelobe responses, with the problematic side-effect of reducing Signal-to-Noise Ratio (SNR).

More recently, processing capabilities that facilitates the viability of back-projection processing techniques as an alternative to transform-based processing removes the imperative for uniform sample spacing. As such, we may directly process purposeful non-uniformly spaced samples in an optimal manner, thereby with their employment mitigating some of the problematic side-effects such as the aforementioned grating lobes and blind velocities, and in some cases even the SNR loss.

With respect to radar signal processing we offer the following background sources.

> Collecting raw SAR data with optimum spatial sampling to facilitate transform-based image formation is discussed in a report by Doerry.[1]
>
> SAR processing using back-projection is described in detail in a report by Doerry, et al.[2]
>
> GMTI processing using back-projection is presented in another report by Doerry.[3]

The conventional approach to resolving Doppler ambiguities is to stagger the Pulse Repetition Frequency (PRF) of the radar, with conventional uniformly spaced samples within the staggered subintervals, if the stagger interval is greater than a single pulse.

Skolnik[4,5] provides in his esteemed books an introduction to designing staggered PRF systems. Extended discussions can also be found in texts by Galati,[6] and by Schleher.[7]

Applying a random "jitter" to the radar PRF has also been investigated, and is discussed by among others Vergara-Dominguez.[8] We note that early investigations often dealt with effects of suboptimal processing of such jittered PRF data.

More recently, techniques have been explored to disambiguate Doppler in GMTI modes by examining residual range migration. Representative publications include those by Xia, et al.,[9] Zhu and Liao,[10,11] and Huang, et al.[12]

The processing of sampled-data is very related to array-antenna design and operation. Much of the mathematics is readily transferable. Aperiodic and random antenna arrays are discussed in some detail in a textbook by Steinberg.[13] Other representative relevant publications include those by Kim and Jaggard,[14] Jarske, et al.,[15] Kumar and Branner,[16] Lo,[17] Lo and Lee,[18] Steinberg,[19] and Unz.[20]

More abstract treatments of non-uniform sampling are available in a number of publications, exemplified by the following.

> An excellent textbook on non-uniform sampling is edited by Marvasti.[21] His text also addresses a number of applications for nonuniform sampling.
>
> Yen[22] examines "some special nonuniform sampling processes" and deduces "some interesting properties of bandwidth-limited signals."
>
> Davis and Lanterman[23] examine aliasing with nonuniform samples.
>
> Aldroubi and Gröchenig[24] discuss "modern techniques for nonuniform sampling and reconstruction of functions in shift-invariant spaces."

We examine herein a more unconstrained sample spacing to facilitate advantage to unambiguously identifying Doppler spectral content.

We note that Legg, et al.,[25] examined using a randomly varying PRF to disambiguate Doppler in a SAR image. Herein we extend these ideas to achieve further-improved performance.

2 Executive Summary

Uniform sample spacing, while particularly “nice” to process, nevertheless exhibits the well-known baggage of aliasing due to grating lobes leading to ambiguous spectrum measurements.

Adjusting sample times to nonuniform spacing interferes with aliasing, and can disambiguate spectral calculations. The nonuniform nature of useful sampling strategies might be deterministic, random, or chaotic.

Proper spectrum calculations must take into account not only the actual nonuniform sample times, but also the local sample spacing at those times. Window taper functions for sidelobe control must also be adjusted to actual sample times.

For radar Doppler analysis, conventional transform-based frequency estimation such as the FFT are inadequate to the task for processing nonuniform-spaced samples. However, the more recent viability of back-projection processing techniques also makes viable the more general calculations necessary for samples with nonuniform spacing.

In some circumstances, the sample spacing itself can be chosen to provide the sidelobe control of window taper functions, so that no additional signal sample amplitude weighting is required. This offers the maximum possible SNR of a spectral response.

"Conformity is the jailer of freedom and the enemy of growth."
-- John F. Kennedy

3 Detailed Discussion

3.1 Some Basics

To set up the following discussion, we begin by defining a generic signal

$$x(t) \text{ = continuous function of time } t. \tag{1}$$

As we will be interested in the Fourier Transform of functions, we accordingly define

$$X(f) = \int_{-\infty}^{\infty} x(t) e^{-j2\pi ft} dt \text{ = forward transform, and}$$

$$x(t) = \int_{-\infty}^{\infty} X(f) e^{j2\pi ft} df \text{ = inverse transform,} \tag{2}$$

where the Fourier Transform is in terms of frequency f. We may use shorthand to identify the transform pair as

$$x(t) \Leftrightarrow X(f). \tag{3}$$

3.2 Periodic (Uniform) Sampling

We now define the periodic sampling function in the conventional manner and identify its transform, namely

$$\sum_n \delta(t - T_s n) \Leftrightarrow f_s \sum_u \delta(f - f_s u), \tag{4}$$

where

n = pulse index,
u = spectral Nyquist band index,
T_s = uniform sampling interval,
$f_s = 1/T_s$ = constant sampling frequency, and
$\delta(z)$ = Dirac delta function. (5)

The individual samples of $x(t)$ are then given (modelled) by

$$x_s(T_s n) = x(t)\delta(t - T_s n) = x(T_s n)\delta(t - T_s n), \tag{6}$$

and the sampled function is identified as

$$x_s(t) = \sum_n x(T_s n)\,\delta(t - T_s n). \tag{7}$$

We will generally assume that we have N samples of the function over an interval of duration T. For uniform periodic samples, we have

$$T = T_s N. \tag{8}$$

Using some identities and theorems, the Fourier Transform of the sampled function is well-known and given by

$$X_s(f) = X(f) * f_s \sum_u \delta(f - f_s u) = f_s \sum_u X(f - f_s u), \tag{9}$$

where "*" denotes convolution.

Digging a little deeper into the Fourier Transform lets us write the specific calculation

$$X_s(f) = \int_{-\infty}^{\infty} \sum_n x(T_s n)\,\delta(t - T_s n) e^{-j2\pi ft} dt, \tag{10}$$

which can be rearranged to

$$X_s(f) = \sum_n \int_{-\infty}^{\infty} x(T_s n)\,\delta(t - T_s n) e^{-j2\pi ft} dt. \tag{11}$$

Performing the integration yields

$$X_s(f) = \sum_n x(T_s n) e^{-j2\pi f T_s n}. \tag{12}$$

This is in fact the Discrete-Time Fourier Transform (DTFT). If we select uniformly spaced sample frequencies, where

$$f = \frac{k}{K} f_s, \tag{13}$$

where

$$K = \text{number of frequency samples over the interval } [0, f_s), \tag{14}$$

then

$$X_s\left(\frac{k}{K}f_s\right)=\sum_n x(T_s n)e^{-j2\pi\frac{k}{K}n}. \tag{15}$$

This is customarily referred to as simply the Discrete Fourier Transform (DFT) of the sequence $x(T_s n)$.

We further note that the DFT is related to the continuous-time spectrum via Eq. (9), such that

$$\sum_u X\left(\frac{k}{K}f_s - f_s u\right)=T_s\sum_n x(T_s n)e^{-j2\pi\frac{k}{K}n}. \tag{16}$$

If $x(t)$ is suitably band-limited, then we may identify the baseband spectrum as

$$X\left(\frac{k}{K}f_s\right)=T_s\sum_n x(T_s n)e^{-j2\pi\frac{k}{K}n}, \tag{17}$$

for suitable values of *k*. What is important to note here is that the calculation of the actual spectrum requires scaling the DFT result by the sampling interval T_s. This is typically 'not' what most implementations of the DFT, such as the Fast Fourier Transform (FFT), in fact calculate.

<u>The Data Interval</u>

We stipulate that we will generally be interested in a finite number of samples over a finite data collection interval. Accordingly, we identify our data characteristics for subsequent analysis as

$$\begin{aligned} &N = \text{number of data samples, with } 0 \le n \le N-1, \text{ and} \\ &T = \text{data collection interval, with individual sample times } 0 \le t_n < T. \end{aligned} \tag{18}$$

These definitions will hold true for the remainder of this report. Nevertheless, for periodic/uniform sampling, we identify

$$T_s = \frac{T}{N}. \tag{19}$$

With malice aforethought, we may also now write the baseband spectrum as

$$X(f)=\frac{T}{N}\sum_n x(t_n)e^{-j2\pi f t_n}. \tag{20}$$

3.3 Aperiodic (Nonuniform) Sampling

Let us now choose arbitrary sampling times such that our sampled function is

$$x_s(t) = \sum_n x(t_n)\delta(t - t_n). \tag{21}$$

We will still generally assume that we have *N* samples of the function over an interval of duration *T*, but the samples at times t_n are no longer required to be uniformly spaced. In antenna array design this may sometimes called a "spatial taper."

The spectrum of this sampled function is then

$$X_s(f) = \int_{-\infty}^{\infty} \sum_n x(t_n)\delta(t - t_n)e^{-j2\pi ft}dt, \tag{22}$$

which can be rearranged to

$$X_s(f) = \sum_n \int_{-\infty}^{\infty} x(t_n)\delta(t - t_n)e^{-j2\pi ft}dt, \tag{23}$$

and then simplified to

$$X_s(f) = \sum_n x(t_n)e^{-j2\pi ft_n}. \tag{24}$$

However, what we really want is an estimate of the continuous-time spectrum $X(f)$. This requires scaling the input signal samples according to their density, which we identify with a "local" sampling frequency and associated "local" sampling period as

$$\begin{aligned} &f_s(t_n) = \text{local sampling frequency, and} \\ &T_s(t_n) = \left[f_s(t_n) \right]^{-1} = \text{local sampling period (interval).} \end{aligned} \tag{25}$$

Note that these are now non-constant functions of t_n. Appendix A in an earlier report offers justification for this.[26] Accordingly, our estimate of a band-limited continuous-time spectrum is identified as

$$X(f) = \sum_n T_s(t_n)x(t_n)e^{-j2\pi ft_n}. \tag{26}$$

We may still choose to index our spectral index to sampled frequencies where

$$f = \frac{k}{K} f_{ref} \,, \tag{27}$$

where now

$$\begin{aligned} K &= \text{number of frequency samples over the interval } [0, f_{ref}) \,, \\ f_{ref} &= \text{a specified reference frequency.} \end{aligned} \tag{28}$$

Since sampling is no longer periodic, we also no longer have the replicated spectra that Eq. (4) would otherwise imply. This means that the aliasing that occurs with uniformly sampled data is subverted, allowing us to discriminate tonal signals beyond what otherwise might be a sampling bandwidth.

We also stipulate that there is no particular reason other than convenience for sampled frequencies to be regular in the frequency domain. We will nevertheless to choose to do so hereafter anyway.

<u>Local Sampling Frequency/Period Calculation</u>

Here we explore the relationship between sample times and the local sampling frequency/period calculations.

Let us begin by defining a reference continuous function for the basis of sampling period calculations as

$$g(z) = \text{some specific differentiable reference function.} \tag{29}$$

Here, the argument z is merely an arbitrary placeholder for now. We further identify that at specific integer arguments

$$g(n) = t_n \,. \tag{30}$$

Essentially, t_n are merely samples of $g(z)$ at integer arguments. Some additional properties include

$$\begin{aligned} &g(0) = 0 \,, \text{ and} \\ &g(N) = T \,. \end{aligned} \tag{31}$$

This allows us to identify the local sampling period as

$$T_s(t_n) = \frac{d}{dz} g(z) \bigg|_{z=n} = g'(z) \big|_{z=n} \,. \tag{32}$$

Otherwise, given the local sampling period, we may identify the sample positions as a summation of previous sampling periods, as we might expect, as

$$t_n \approx \sum_{m=0}^{n-1} T_s\left(t_m\right). \tag{33}$$

This is only approximate due to the vagaries inherent in sample-time increments not being precisely equal to the local sampling period at a particular sample time. This difference diminishes for smooth functions as the number of sample times increases.

Often, we will choose a $g'(z)$, but such that

$$\int_{z=0}^{N} g'(z)dz = T, \tag{34}$$

and therefrom calculate $g(z)$. Occasionally, however, we may in fact begin with $g(z)$ and therefrom identify $g'(z)$. Sometimes, iteration between the two might even be required.

In any case, once we have a $g(z)$ and $g'(z)$ pair, we may use Eq. (30) and Eq. (32) to identify both sample times and local sampling period. This is what we want.

We note that our choice of *N* samples in *T* seconds remains consistent with the case of uniform sampling. That is, we are not seeking advantage by increasing either of these over the uniform sampling case. We are merely rearranging the specific sample times to no longer be uniform.

Comments

Marvasti[21] addresses the question "Under what conditions do the nonuniform samples represent a signal uniquely?" He answers with the following lemma, attributed to Requicha[27].

> Lemma for 1-D Signals: If the nonuniform samples $\{t_n\}$ satisfy the Nyquist rate on the average, it can uniquely represent a band-limited signal (deterministic or random) if the samples are not the zero-crossings of a band-limited signal of the same bandwidth. The set $\{t_n\}$ is then called a sampling set.

We understand from this that as long as the "average" sampling rate is not diminished, then nonuniform sampling offers no loss in information compared to uniform samples for band-limited signals.

3.4 Aperiodic (Nonuniform) Sampling with Window Tapers

Window taper functions are used in processing data to control processing sidelobe characteristics. There are many windows from which to choose, with various trades in parameters and characteristics.[28]

To facilitate using window taper functions with aperiodic data samples, we need to define the window functions in a manner other than uniformly spaced samples. Let us define a window function in terms of a continuous function, namely

$$w\left(\frac{t}{T}-\frac{1}{2}\right). \tag{35}$$

The window functions we shall consider typically (although exceptions exist) have the following convenient properties.

1. $w(z)$ is real, even, and typically positive. Argument z is an arbitrary placeholder.

2. $w(z)$ is of finite length, defined over the interval $[-1/2, 1/2]$, with

$$w(z) = w(z)\,\mathrm{rect}(z). \tag{36}$$

   We stipulate $w(z)$ is zero outside of the interval $[-1/2, 1/2]$.

3. $w(z)$ has unit DC gain. This means

$$\int_{-\infty}^{\infty} w(z)\,dz = 1. \tag{37}$$

   This also means that if any part of $w(z)$, edges notwithstanding, is less than one, then $w(0) > 1$.

4. $w(z)$ is typically non-increasing with distance from its center. This means

$$w(z_1) \geq w(z_2) \text{ for } |z_1| < |z_2|. \tag{38}$$

An example of such a window taper function is the Hann (a.k.a. Hanning) window, stipulated to be

$$w(z) = \left(1 + \cos(2\pi z)\right)\mathrm{rect}(z), \tag{39}$$

where

$$\text{rect}\left(z\right)=\begin{cases}1 & \left|z\right|\le 1/2\\ 0 & else\end{cases}. \tag{40}$$

Employing such a window function modifies our estimate of the band-limited continuous-time spectrum to

$$X\left(f\right)=\sum_{n} w\left(\frac{t_n}{T}-\frac{1}{2}\right)T_s\left(t_n\right)x\left(t_n\right)e^{-j2\pi f t_n}. \tag{41}$$

Of course we may continue to index this to sampled frequencies where, as before

$$f=\frac{k}{K}f_{ref}. \tag{42}$$

We observe that to estimate the band-limited continuous-time spectrum in Eq. (41), the specific data samples are weighted with two distinct factors. The first is the local sampling period $T_s\left(t_n\right)$, and the second is the actual taper function $w\left(t_n/T-1/2\right)$. These two factors combine for a net data weighting being their product $\left[w\left(t_n/T-1/2\right)T_s\left(t_n\right)\right]$.

Special Case

Consider the case where the variations in the two weighting factors 'cancel' each other, that is, we now let

$$w\left(\frac{t_n}{T}-\frac{1}{2}\right)T_s\left(t_n\right)=\frac{T}{N}\quad\text{for all } t_n. \tag{43}$$

This of course implies that the local sampling frequency equals the local window weighting appropriately scaled, namely

$$f_s\left(t_n\right)=\frac{N}{T}w\left(\frac{t_n}{T}-\frac{1}{2}\right)\quad\text{for all } t_n. \tag{44}$$

More generally, we can identify the reference function and its derivative by solving the differential equation

$$g'\left(z\right)=\frac{T/N}{w\left(\dfrac{g\left(z\right)}{T}-\dfrac{1}{2}\right)}\quad\text{for all } 0\le z<N. \tag{45}$$

We acknowledge this is not trivial. The following iterative numerical technique borrowed from an earlier report on Non-Linear FM (NLFM) chirp generation may be used to calculate the required functions.[29]

1. Initialize $g'(z) = T/N$.
2. Integrate $g'(z)$ to calculate $g(z)$.
3. Scale $g'(z)$ and $g(z)$ to meet the T constraint of Eq. (31).
4. Calculate $w\left(\frac{g(z)}{T} - \frac{1}{2}\right)$, and therefrom $g'(z)$ using Eq. (45).
5. Repeat steps 2-5 until convergence.

Nevertheless, from this solution we may use Eq. (30) and Eq. (32) to identify both sample times and local sampling period.

Having done this, Eq. (43) will hold, thereby allowing a "windowed" DFT result by reducing Eq. (41) to simply

$$X(f) = \frac{T}{N}\sum_n x(t_n)e^{-j2\pi f t_n} \,. \tag{46}$$

That is, the data can be simply added with appropriate phase shift, and no overt amplitude tapering, and 'still' achieve processing sidelobe reduction. From Appendix A, we also understand this to be the optimum SNR result.

A caveat is that any window taper functions used in Eq. (45) cannot go to zero, and probably shouldn't even approach very near to zero. For example, the Hann window of Eq. (39) would not be a very good candidate for this.

We further suggest that any sample spacing and window taper function combination that brings $\left[w(t_n/T - 1/2)T_s(t_n)\right]$ closer to Eq. (43) will generally improve SNR, even if Eq. (43) cannot be exactly achieved.

An interesting viewpoint is that there are actually two window taper functions to consider. The first is the equivalent taper function due to $T_s(t_n)$ alone, and the second is the net desired window taper function to yield the final spectrum characteristic.

3.5 Aperiodic Sample Times Selection

Given the analysis in the previous sections, we summarize with the following procedure for selecting the sample times.

1. Select one of the functions $g'(z)$ and $g(z)$ for a desired characteristic, and calculate the other, both subject to the constraints in Eq. (31). The function $g'(z)$ may also need to be constrained to greater than some minimum value in consideration of range ambiguities.

2. From the functions $g'(z)$ and $g(z)$, calculate the sample times t_n and local sample spacing $T_s(t_n)$ at those times, using Eq. (30) and Eq. (32).

For subsequent spectral analysis of the sampled signal, we might add the following steps.

3. Choose a final net window taper function $w(z)$.

4. Calculate the signal spectrum using Eq. (41), perhaps at specific frequencies using Eq. (42).

4 Sampling Strategies

We now examine several sampling strategies.

In all subsequent cases, we expect common parameters for the following.

$$\begin{aligned} &N = \text{number of data samples, with } 0 \le n \le N-1, \text{ and} \\ &T = \text{data collection interval, with } 0 \le t_n < T. \end{aligned} \tag{47}$$

Note that the "average" sampling rate will be held constant. In particular, for the following examples, we will assume $N = 1024$, and $T = 0.25$ s. To illustrate signal processing fidelity, we will also assume a noise-free signal with unit amplitude with arbitrarily chosen frequency of $0.25\,N/T$. Specifically, our input test signal is

$$x(t) = e^{j2\pi[0.25\,N/T]t} = \text{arbitrary test signal.} \tag{48}$$

Unless indicated otherwise, we will also assume employment of a Hann window taper function.

4.1 Constant Sample Spacing (Reference)

To provide reference for following aperiodic sampling strategies, we begin with the conventional uniform sampling, conducive to FFT processing, where

$$\begin{aligned} g'(z) &= \frac{T}{N} = \text{constant sample time increments, and} \\ g(z) &= \frac{T}{N} z = \text{linear increment in sample times.} \end{aligned} \tag{49}$$

For this first sampling of our reference signal we choose a constant PRF; a constant sample time increment. This is the conventional sampling strategy. Furthermore, we will begin with no window taper function.

Figure 1 shows the sample-time increment as a function of essentially sample index. Note that this is constant. Figure 2 shows the spectrum of the signal. Note that for a uniform sampling strategy, we have replicated spectra at integer offsets of the constant PRF; these offset intervals being multiples of N/T. These grating lobes are well-understood. Otherwise, the structure of the response is precisely what we expect for using no window taper function, namely a sinc-like response. Figure 3 is a zoomed version of the mainlobe response, showing the associated high sidelobes.

If we use the same sampling strategy, but with a Hann window taper function, the plots are modified to those of Figure 4 through Figure 6. Note the sidelobe reduction, albeit at the expense of a slightly broadened mainlobe.

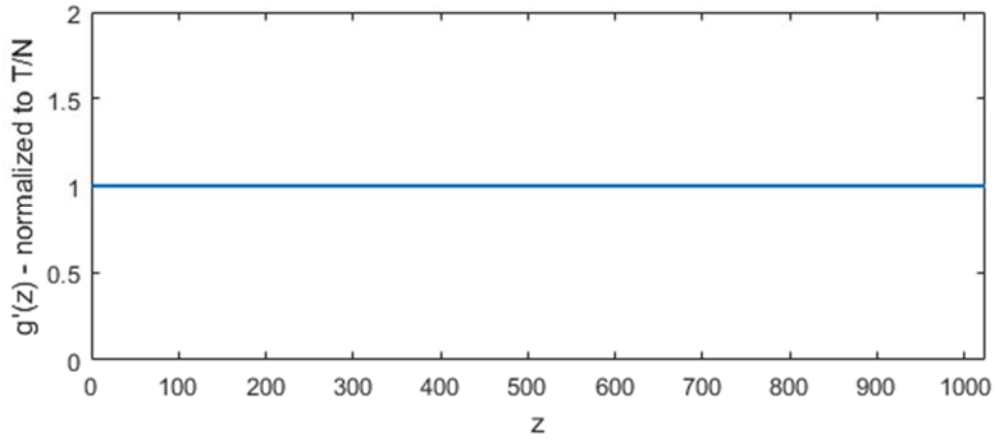

Figure 1. Sample-time increments normalized to *T/N*.

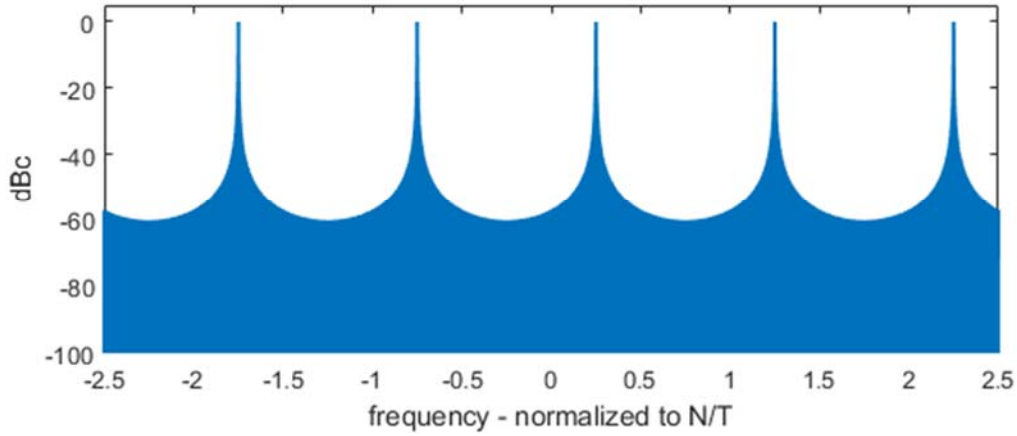

Figure 2. Spectrum of input signal with Uniform tapering.

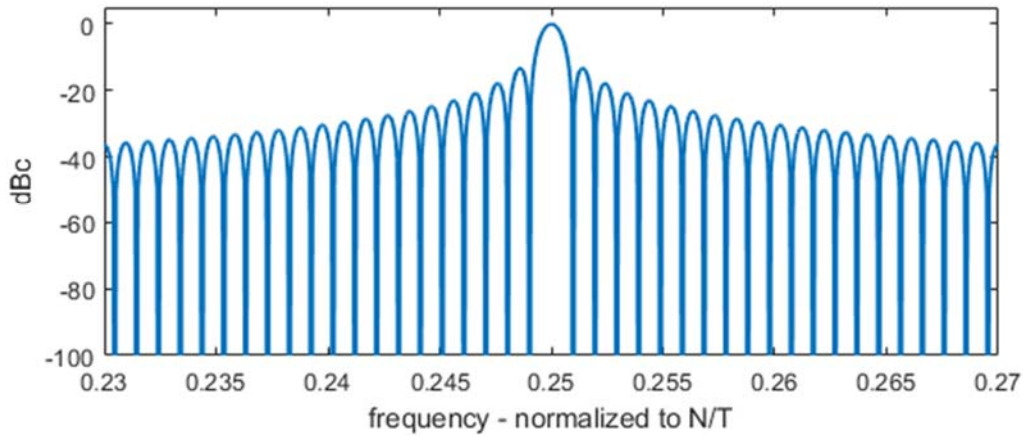

Figure 3. Zoomed rendering of Figure 2.

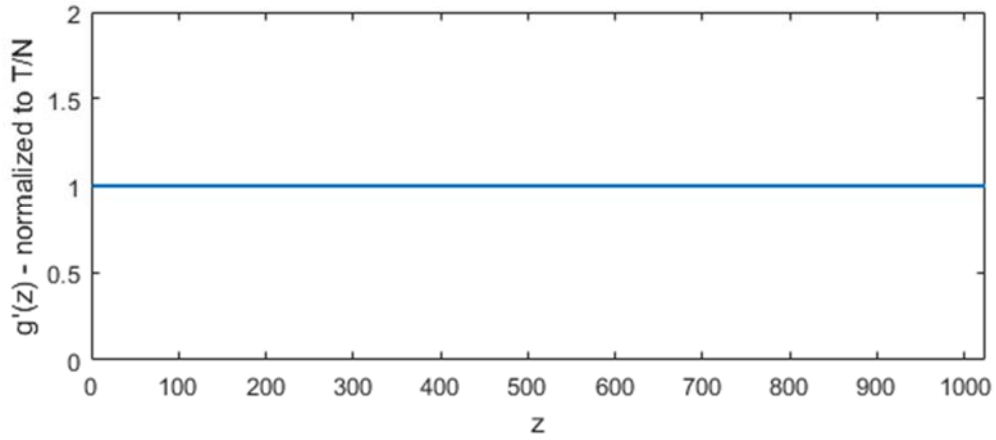

Figure 4. Sample-time increments normalized to *T/N*.

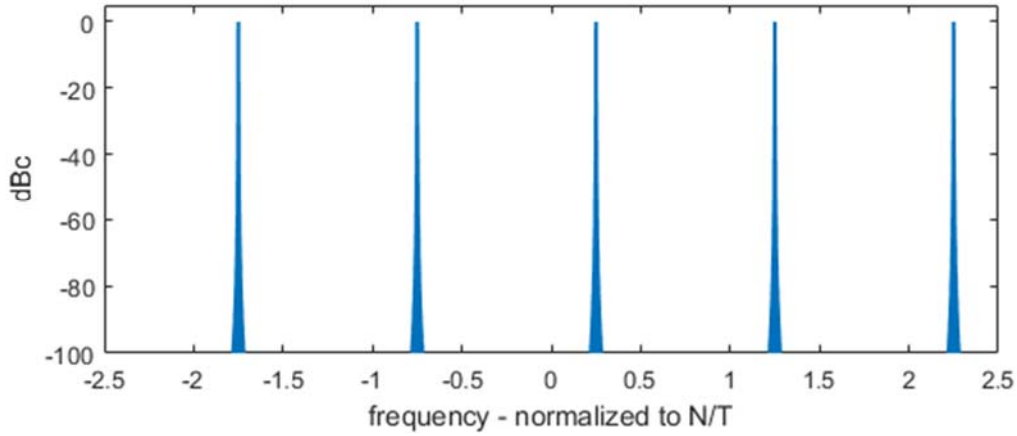

Figure 5. Spectrum of input signal using Hann window taper function.

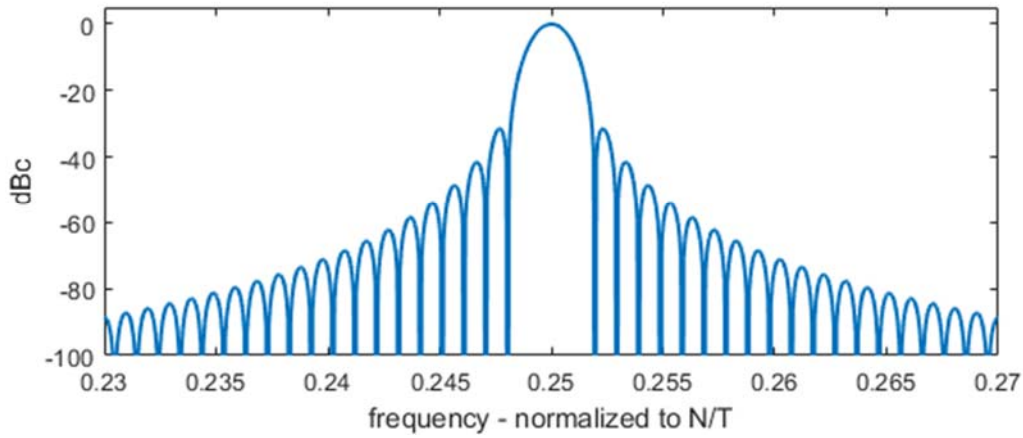

Figure 6. Zoomed rendering of Figure 5.

4.2 Staggered/Stepped Sample Spacing

A not-uncommon practice to disambiguate Doppler frequency is to stagger the radar PRF. This involves dividing the overall observation interval into multiple subintervals, with each sub-interval operating at a unique PRF. The information from the subintervals are then combined or compared to ascertain the proper Doppler estimate.

We exemplify this technique by dividing the N pulses into four groups, each with an equal-number of pulses, and with the sample time increments illustrated in Figure 7. While various schemes can be concocted for how the spectra from the individual subintervals are combined, we shall combine the data coherently for a single spectrum response.

As we might expect, and as shown in Figure 8, we still have a maximum response at the correct signal frequency, but the regular grating lobes previously exhibited in Figure 5 have now had their energy divided into lesser grating lobes corresponding to aliasing due to the individual PRFs of the subintervals. Furthermore, the lesser lobes are broader as well. We do note that while the lesser grating lobes are reduced, some are still quite strong.

For this reason, a more typical operating procedure would be to coherently process each subinterval separately, rather than as one single data set. Separate detections for the various subintervals would be compared, passing only those that coincided. This amounts to a voting scheme, or non-coherent filtering of the subinterval results. Since coherent processing is only over a subinterval, there is an attendant SNR loss, especially for low-SNR signals.

As the number of subintervals increases, we would observe a corresponding increase in the number of lesser grating lobes, but the strength of the individual aliased components would themselves decrease.

We note that the stagger need not be generally increasing, and can in fact be randomly ordered. Furthermore, the specific PRF of the subintervals also need not be regularly spaced, nor do the lengths of the subintervals need be equal in time or in number of pulses.

Figure 10 through Figure 12 illustrate a set of randomly chosen PRFs for each of four subintervals.

Figure 13 through Figure 15 illustrate a set of randomly chosen PRFs for each of 64 subintervals, with each subinterval of length 16 pulses. Note that the proper mainlobe response remains nice and clean.

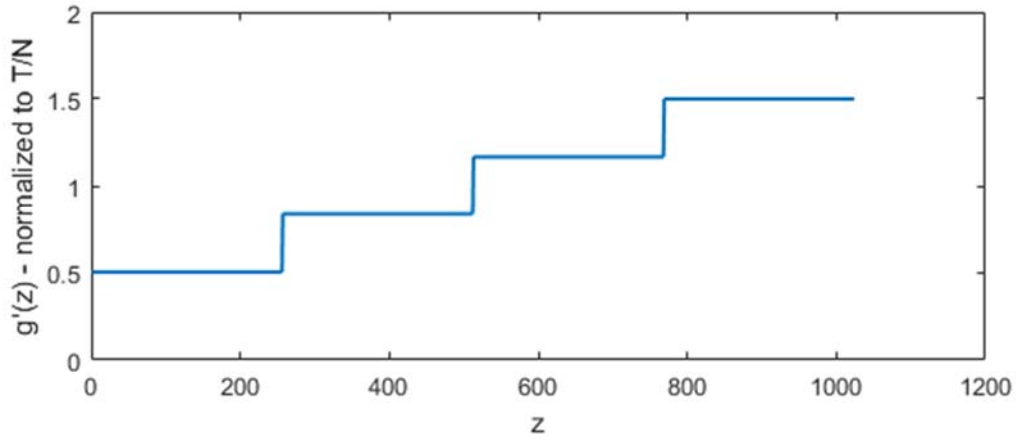

Figure 7. Sample-time increments normalized to *T/N*.

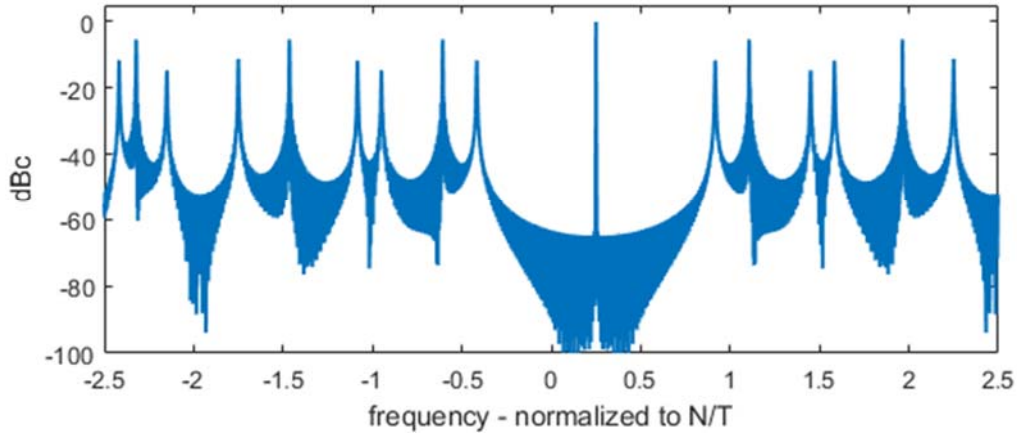

Figure 8. Spectrum of input signal using Hann window taper function.

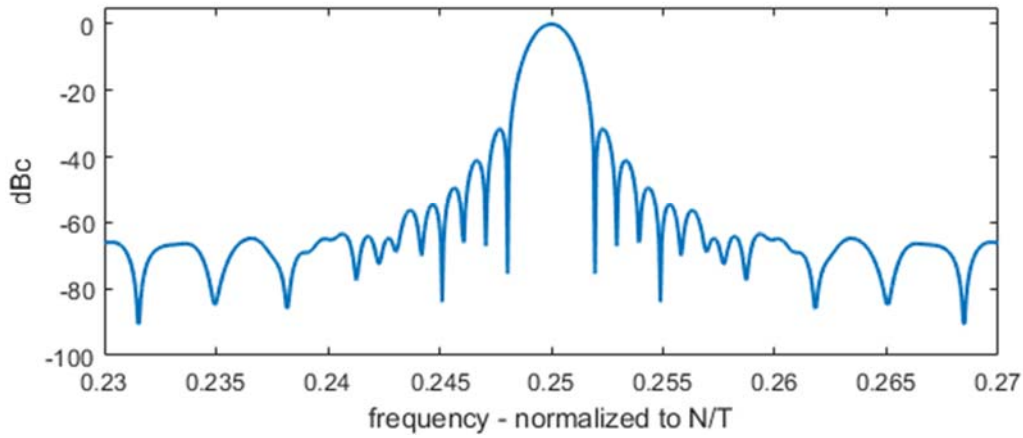

Figure 9. Zoomed rendering of Figure 8.

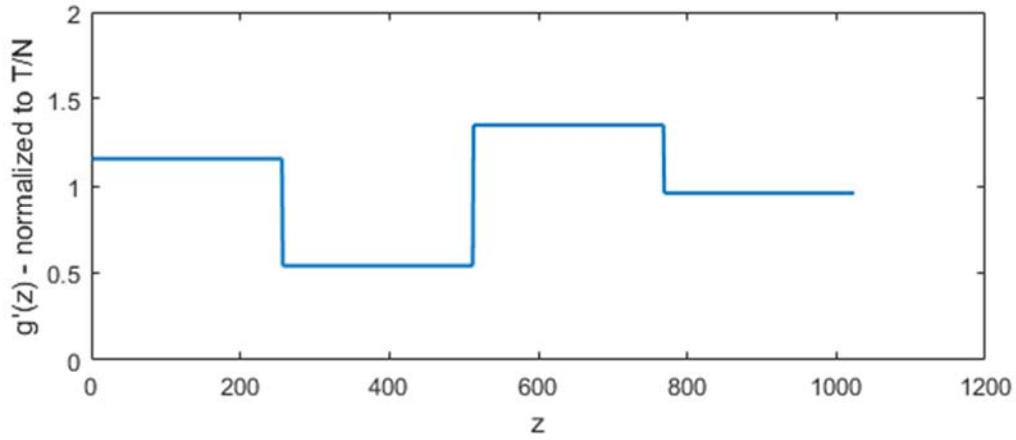

Figure 10. Sample-time increments normalized to *T/N*.

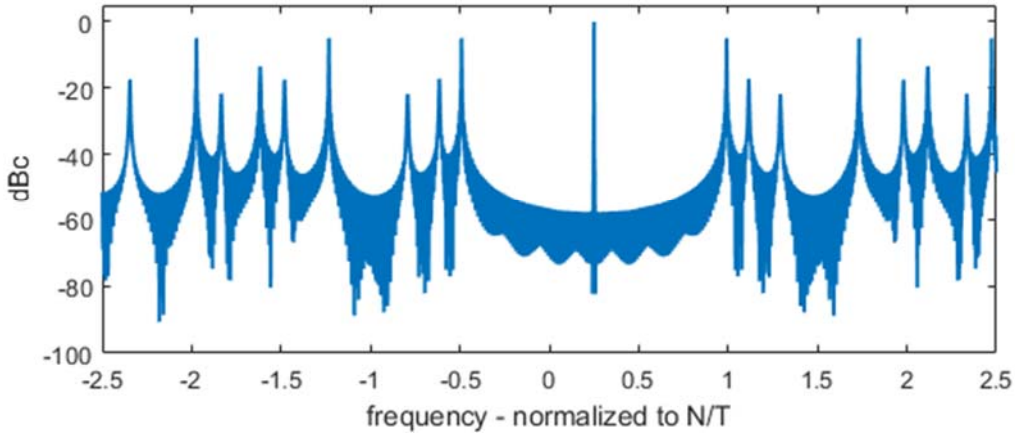

Figure 11. Spectrum of input signal using Hann window taper function.

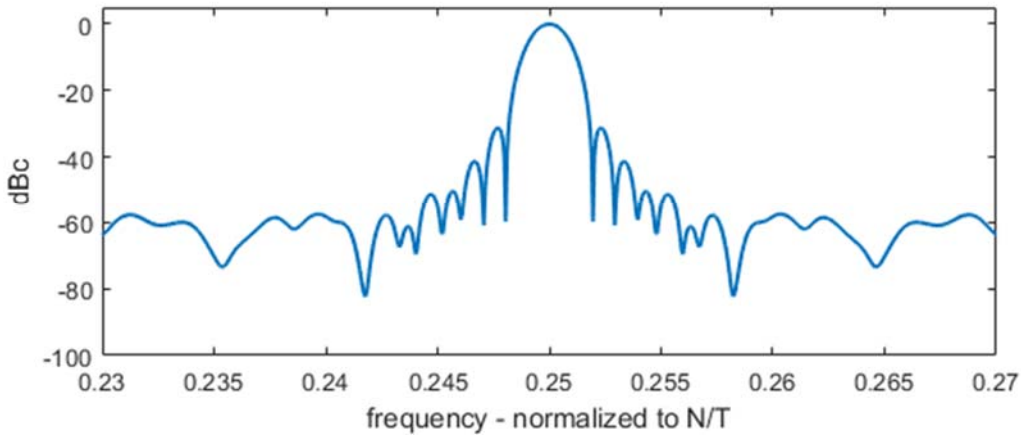

Figure 12. Zoomed rendering of Figure 11.

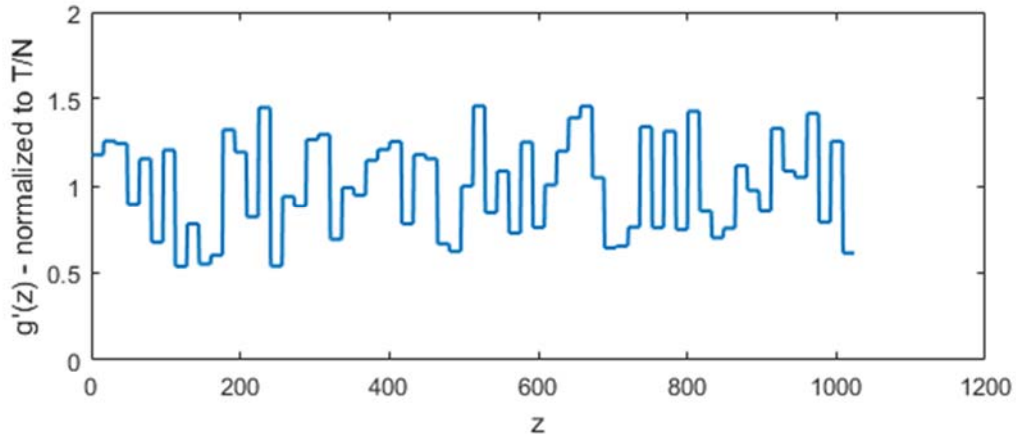

Figure 13. Sample-time increments normalized to *T/N*.

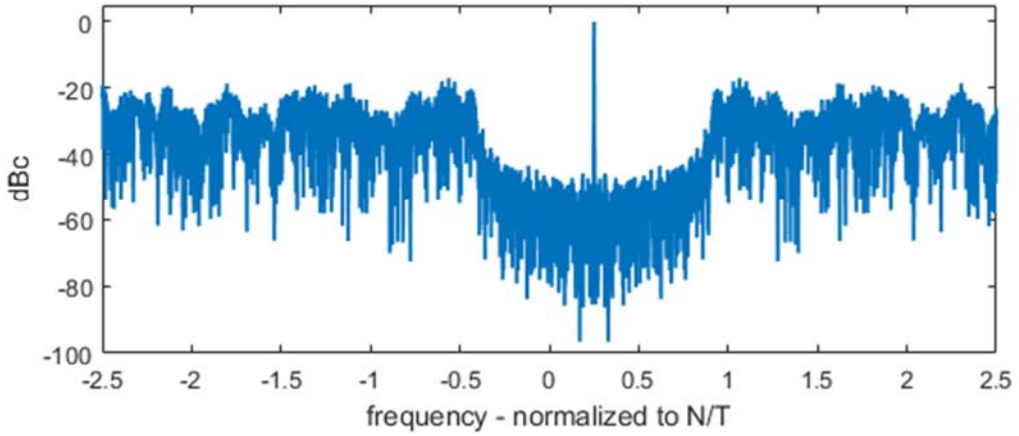

Figure 14. Spectrum of input signal using Hann window taper function.

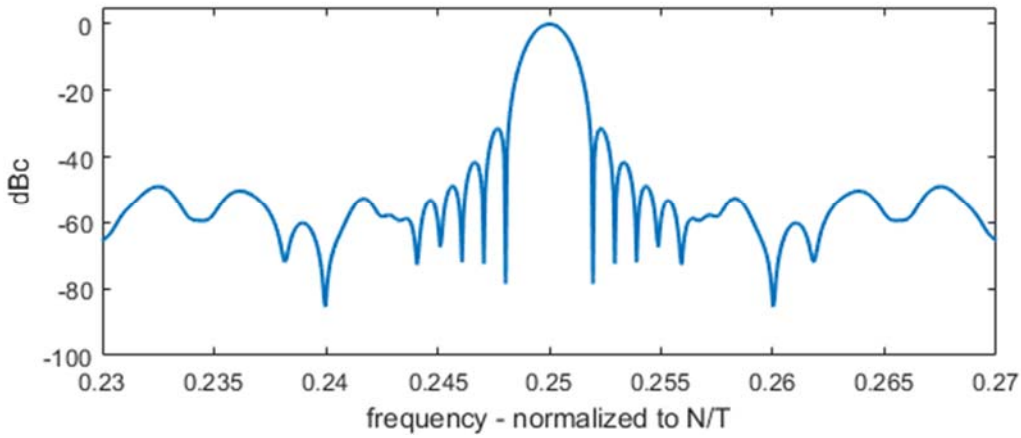

Figure 15. Zoomed rendering of Figure 14.

4.3 Linear-Chirped Sample Spacing

We now examine a "linear-chirped" sample spacing; a sample spacing where the sample time increments change with each pulse in a linear manner. Specifically, we construct

$$g'(z) = \frac{T}{N}\left[\left(1-\frac{a}{2}\right)+\frac{a}{N}z\right] = \text{sample time increments, and}$$
$$g(z) = \frac{T}{N}\left[\left(1-\frac{a}{2}\right)z+\frac{a}{2N}z^2\right] = \text{sample times,} \tag{50}$$

where

$$a = \text{the variation of } g'(z) \text{ with respect to } T/N\,. \tag{51}$$

Figure 16 illustrates the case of $g'(z)$ with $a = 1$. Note its linear ramp.

Figure 17 shows the spectrum of the input signal so sampled, with the additional sample scaling of a Hann window taper function. Figure 18 details the mainlobe response and near-in sidelobes. We note that in spite of nonuniform sampling, that the spectral response is virtually perfect for the mainlobe and a significant bandwidth around the mainlobe, in fact a region greater than N/T.

We also note that the grating lobes evident in Figure 5 are absent, having been replaced by broadly smeared versions thereof with attendant reductions of at least 22 dB in this example. The reduction furthers as *N* increases. The coherence of any energy that otherwise might have been aliased in Doppler has essentially been severely diminished.

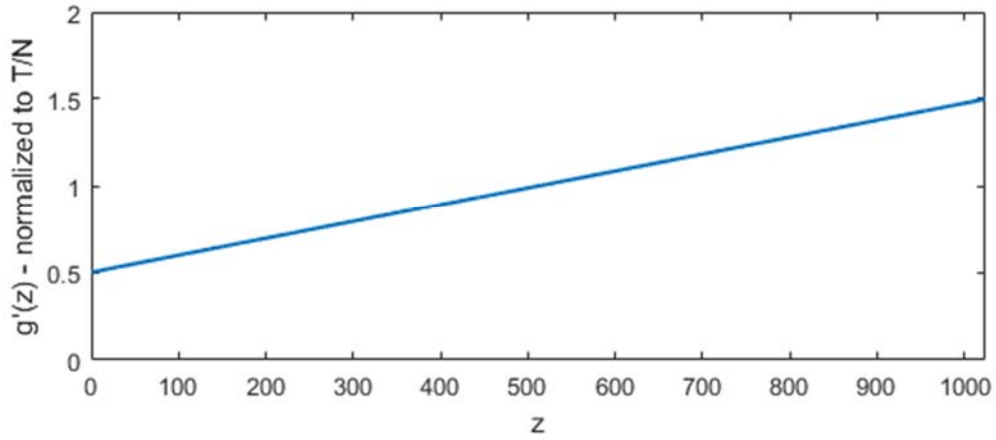

Figure 16. Sample-time increments normalized to *T/N*.

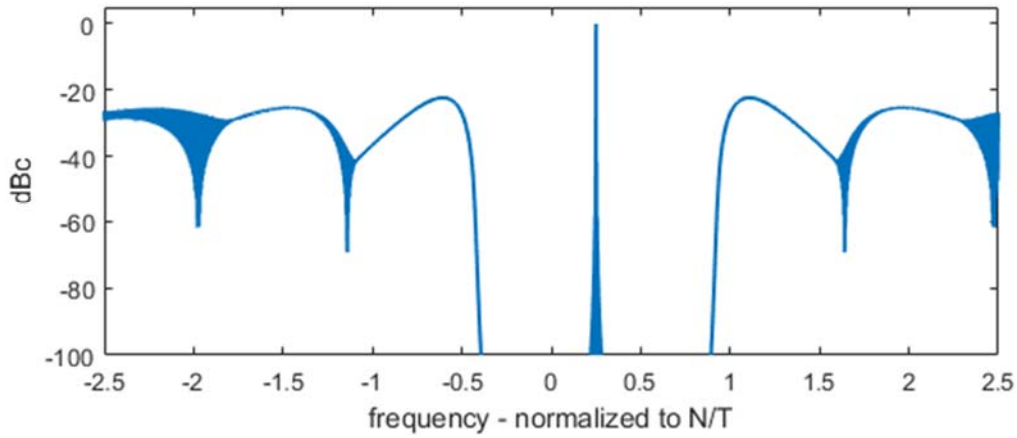

Figure 17. Spectrum of input signal using Hann window taper function.

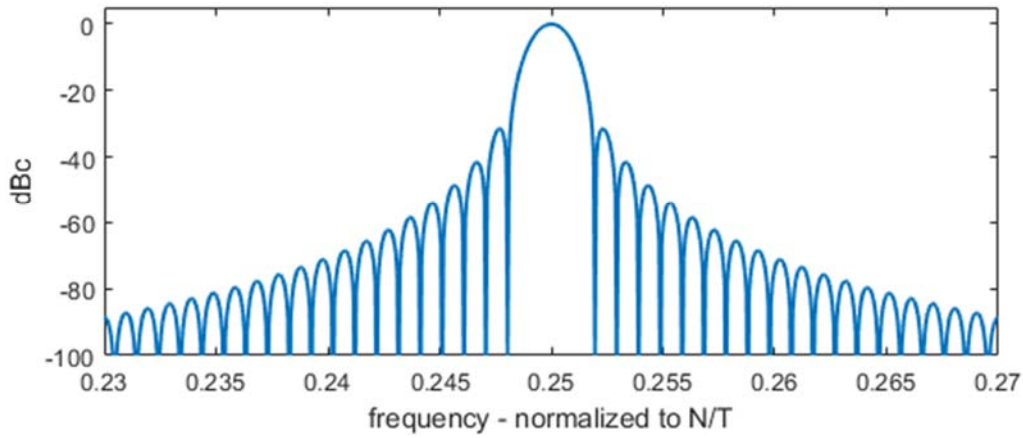

Figure 18. Zoomed rendering of Figure 17.

4.4 Sinusoidal Sample Spacing

We now examine a "sinusoidal" sample spacing; a sample spacing where the sample time increments change with each pulse in a sinusoidal manner. Specifically, we construct

$$g'(z) = \frac{T}{N}\left[1 + \frac{a}{2}\cos\left(\frac{2\pi}{N}z\right)\right] = \text{sample time increments, and}$$
$$g(z) = \frac{T}{N}\left[z + \frac{aN}{4\pi}\sin\left(\frac{2\pi}{N}z\right)\right] = \text{sample times,} \tag{52}$$

where

$$a = \text{the peak-to-peak variation of } g'(z) \text{ with respect to } T/N\,. \tag{53}$$

Figure 19 illustrates the case of $g'(z)$ with $a = 1$. Note its sinusoidal nature.

Figure 20 shows the spectrum of the input signal so sampled, with the additional sample scaling of a Hann window taper function. Figure 21 details the mainlobe response and near-in sidelobes. We note that in spite of nonuniform sampling, that the spectral response is virtually perfect for the mainlobe and a significant bandwidth around the mainlobe, in fact a region greater than N/T.

We also note that the grating lobes evident in Figure 5 are absent, having been replaced by a number of lesser sidelobes with attendant reductions of at least 19 dB in this example. The reduction furthers as *N* increases. The coherence of any energy that otherwise might have been aliased in Doppler has essentially been severely diminished.

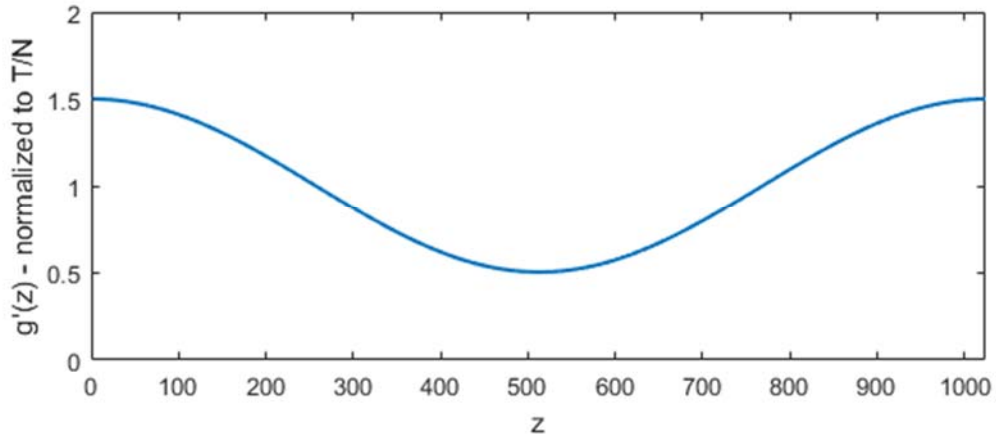

Figure 19. Sample-time increments normalized to *T/N*.

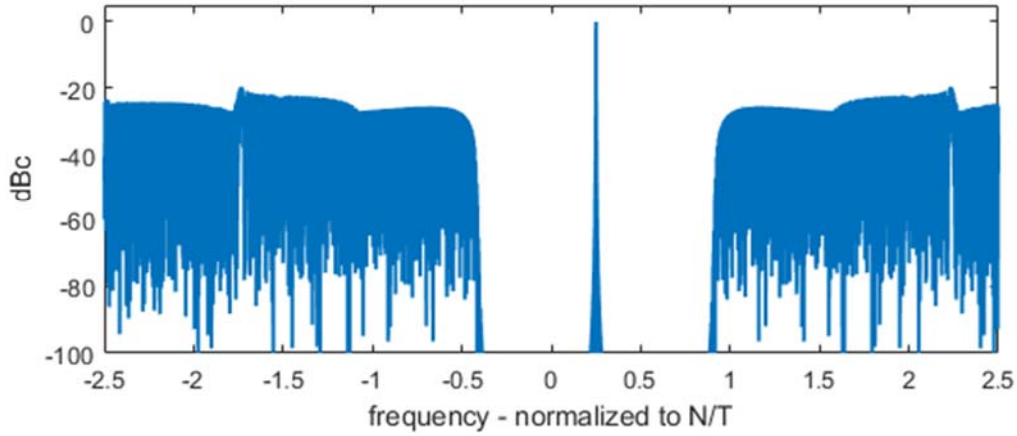

Figure 20. Spectrum of input signal using Hann window taper function.

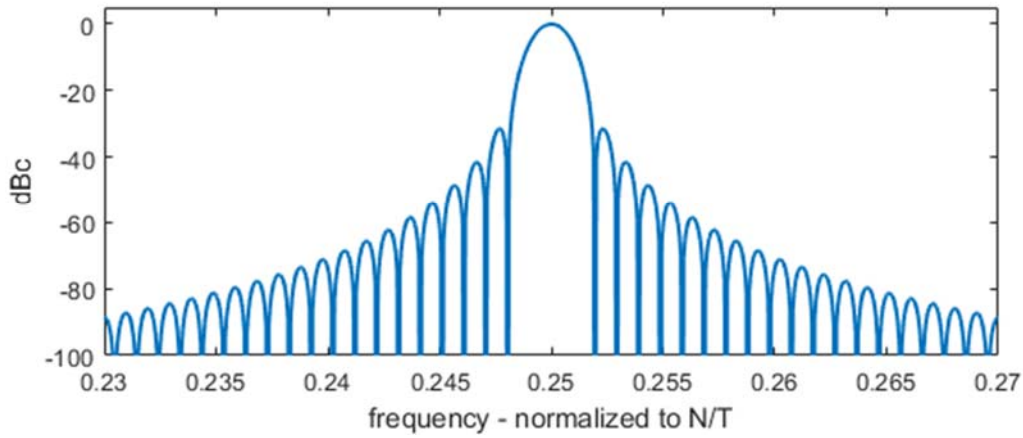

Figure 21. Zoomed rendering of Figure 20.

4.5 Log-Periodic Sample Spacing

We now examine a "log-periodic" sample spacing; a sample spacing where the sample time increments change with each pulse in an exponential manner, i.e. where the log of the sample spacing is periodic. Specifically, we construct

$$g'(z) = \frac{T}{N}\left[b e^{az} \right] = \text{sample time increments, and}$$
$$g(z) = \frac{T}{N}\left[\frac{b}{a} e^{az} - \frac{b}{a} \right] = \text{sample times,} \tag{54}$$

where

$$\begin{aligned} b &= \text{the initial minimum sample spacing,} \\ a &= \text{the exponential growth rate of the sample time increments.} \end{aligned} \tag{55}$$

Note that Eq. (31) requires that a be found to satisfy

$$g(N) = T. \tag{56}$$

Figure 22 illustrates the case of $g'(z)$ with $b = 1/2$, and $a = 0.001228$.

Figure 23 shows the spectrum of the input signal so sampled, with the additional sample scaling of a Hann window taper function. Figure 24 details the mainlobe response and near-in sidelobes. We note that in spite of nonuniform sampling, that the spectral response is virtually perfect for the mainlobe and a significant bandwidth around the mainlobe, in fact a region greater than N/T.

We also note that the grating lobes evident in Figure 5 are absent, having been replaced by broadly smeared versions thereof with attendant reductions of at least 23 dB in this example. We observe that this is somewhat better than the example of Figure 17, although the smearing is slightly broader. The reduction furthers as N increases. The coherence of any energy that otherwise might have been aliased in Doppler has again essentially been severely diminished.

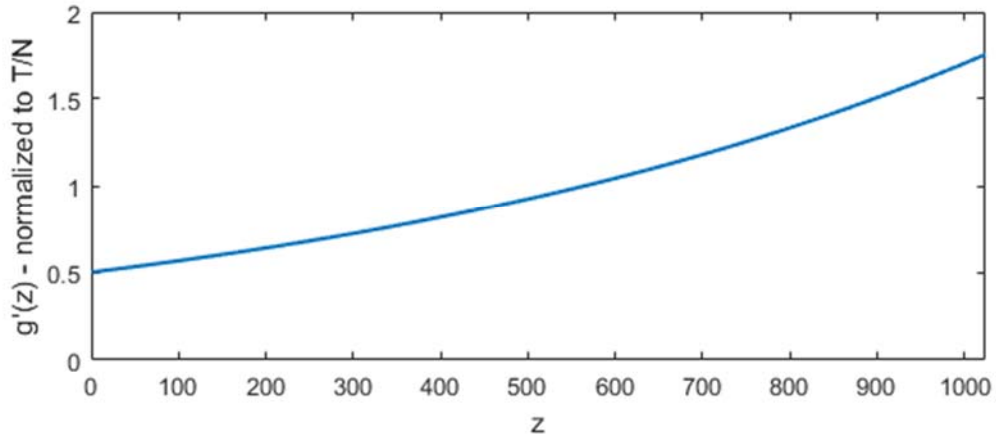

Figure 22. Sample-time increments normalized to *T/N*.

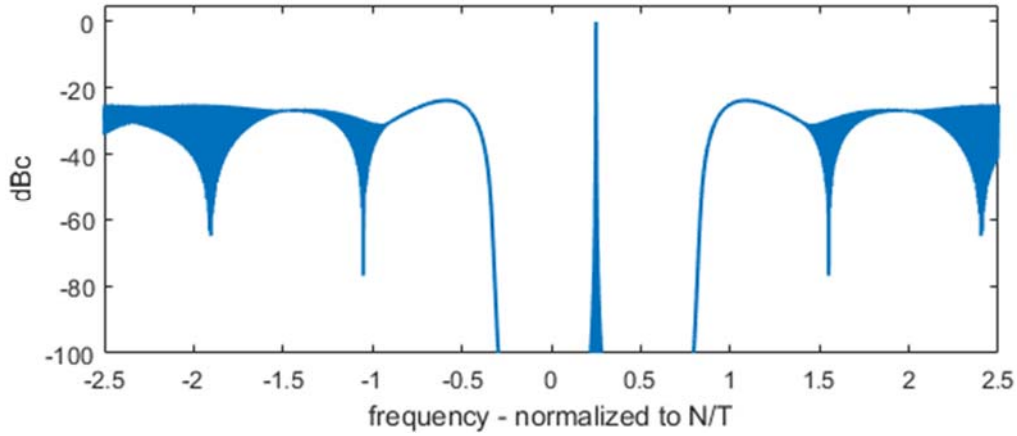

Figure 23. Spectrum of input signal using Hann window taper function.

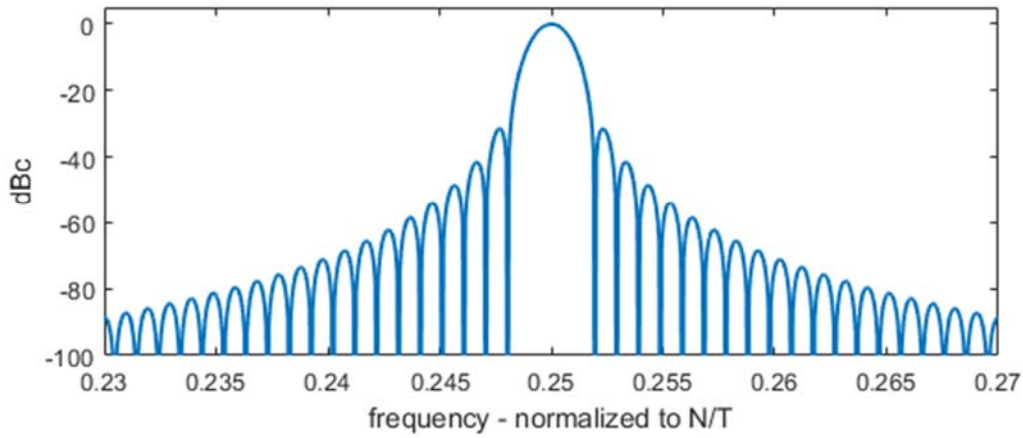

Figure 24. Zoomed rendering of Figure 23.

4.6 Random Sample Spacing

We now examine a random sample spacing; a sample spacing constructed from a random process. Specifically, we arbitrarily generate a 9th order polynomial with random coefficients. There is nothing special about this process except that in spite of its randomness, it is still smooth.

Our process is to generate the random polynomial to give us $g'(z)$, and then integrate to give us $g(z)$. The resulting function is scaled and shifted to satisfy Eq. (31).

Figure 25 illustrates a resulting $g'(z)$.

Figure 26 shows the spectrum of the input signal so sampled, with the additional sample scaling of a Hann window taper function. Figure 27 details the mainlobe response and near-in sidelobes. We note that in spite of nonuniform sampling, that the spectral response is virtually perfect for the mainlobe and a significant bandwidth around the mainlobe, in fact excellent over a region greater than N/T.

We also note that the grating lobes evident in Figure 5 are still absent, having been replaced by broadly smeared versions thereof with attendant reductions of at least 23 dB in this example. The coherence of any energy that otherwise might have been aliased in Doppler has again essentially been severely diminished.

Any of a number of random or chaotic functions might generate suitable sample spacings, provided that results are scaled/shifted to satisfy Eq. (31). Smoothness, essentially a high degree of correlation from one sample to the next, is a desirable trait.

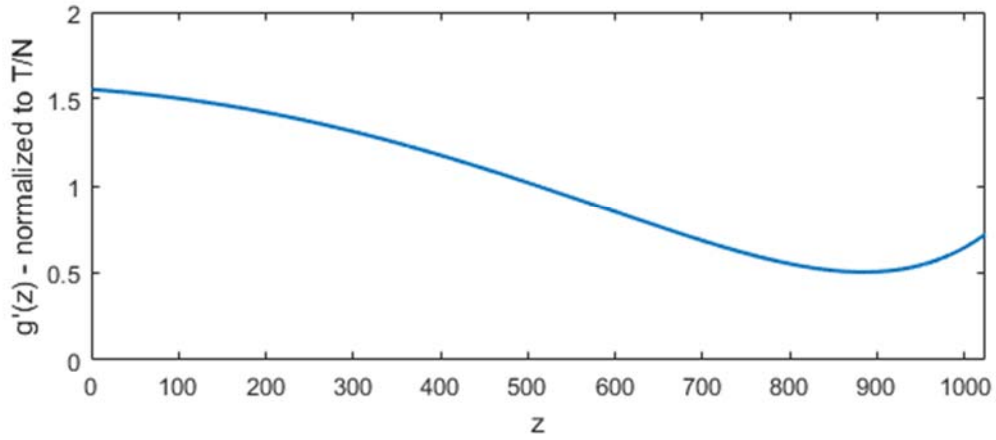

Figure 25. Sample-time increments normalized to *T/N*.

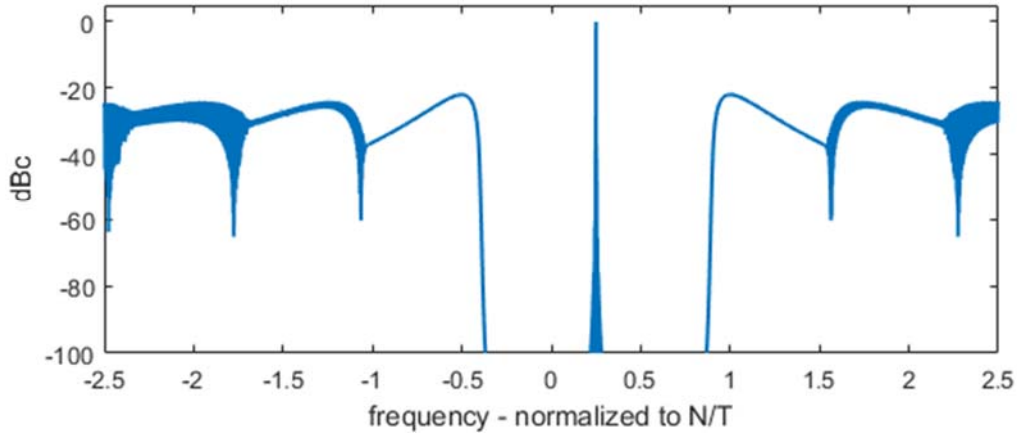

Figure 26. Spectrum of input signal using Hann window taper function.

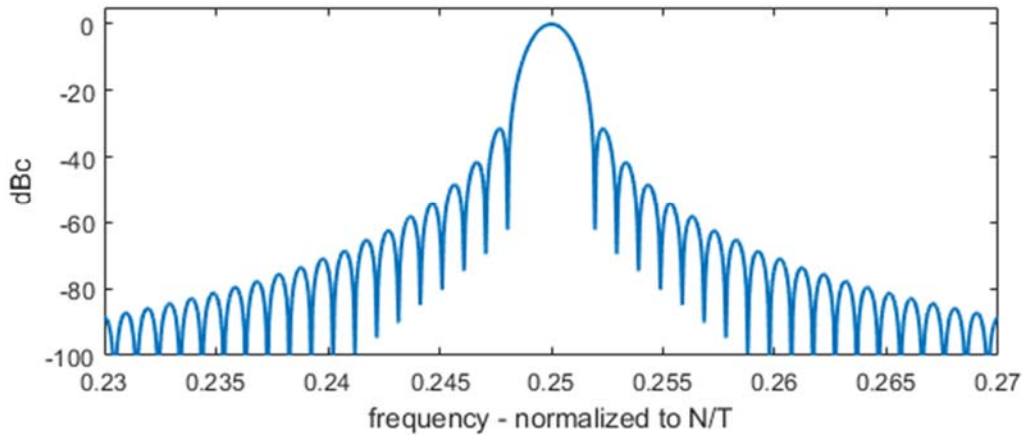

Figure 27. Zoomed rendering of Figure 23.

4.7 Sample Spacing for Sidelobe Control with Maximum SNR

As discussed in section 3.4, sample spacing may be selected in some cases to effect a particular window taper function.

We now examine a sample spacing calculated to yield a spectrum identical to that of a Hamming window without any additional amplitude weighting, for which we identify

$$w(z) = \left(1 + \frac{(1-\alpha)}{\alpha}\cos(2\pi z)\right)\mathrm{rect}(z), \tag{57}$$

with $\alpha = 25/46$ for a Hamming window function. Specifically, we recall Eq. (45), and stipulate

$$g'(z) = \frac{T/N}{w\left(\frac{g(z)}{T} - \frac{1}{2}\right)} \quad \text{for all } 0 \le z < N. \tag{58}$$

Using the procedure outlined in section 3.4, we numerically calculate $g(z)$ accordingly.

Figure 28 illustrates $g'(z)$ to yield the Hamming window characteristic.

Figure 29 shows the spectrum of the input signal so sampled, with no additional amplitude scaling by either sample spacing or window taper function. Figure 30 details the mainlobe response and near-in sidelobes. We note that the nonuniform sampling alone achieved a spectral response that is virtually perfect for the mainlobe and some bandwidth around the mainlobe. We do observe that the region of good agreement is somewhat less than the N/T bandwidth of previous examples.

Nevertheless, we still note that the grating lobes evident in Figure 5 are absent, having been replaced by broadly smeared versions thereof with attendant reductions. The reduction furthers as *N* increases. The coherence of any energy that otherwise might have been aliased in Doppler has again essentially been severely diminished, the aforementioned diminished region of good agreement with Hamming window spectrum notwithstanding.

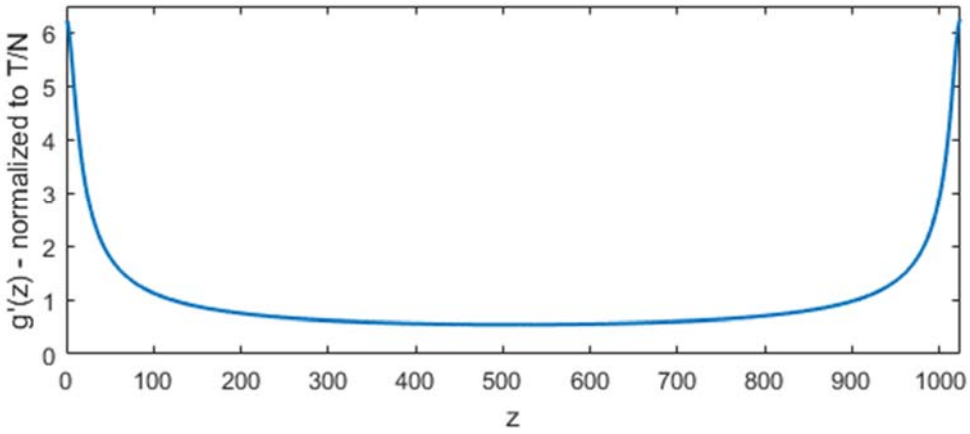

Figure 28. Sample-time increments normalized to *T/N*.

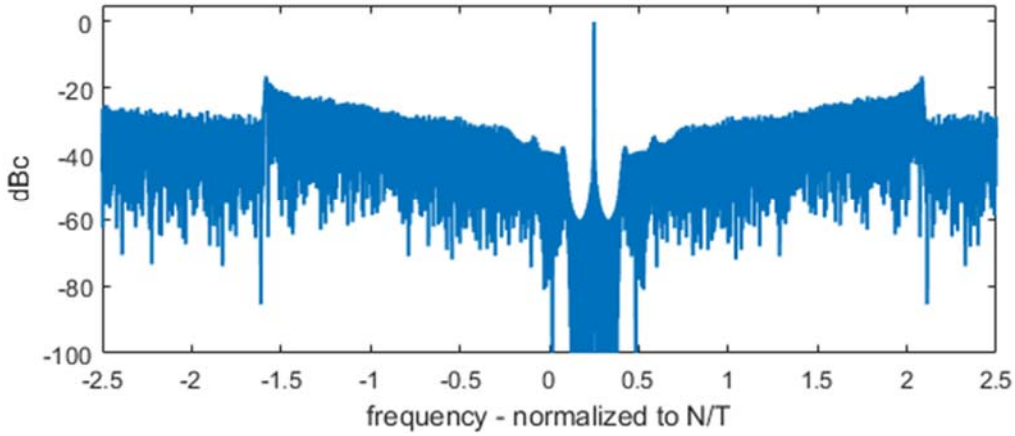

Figure 29. Spectrum of input signal using Hamming window taper function.

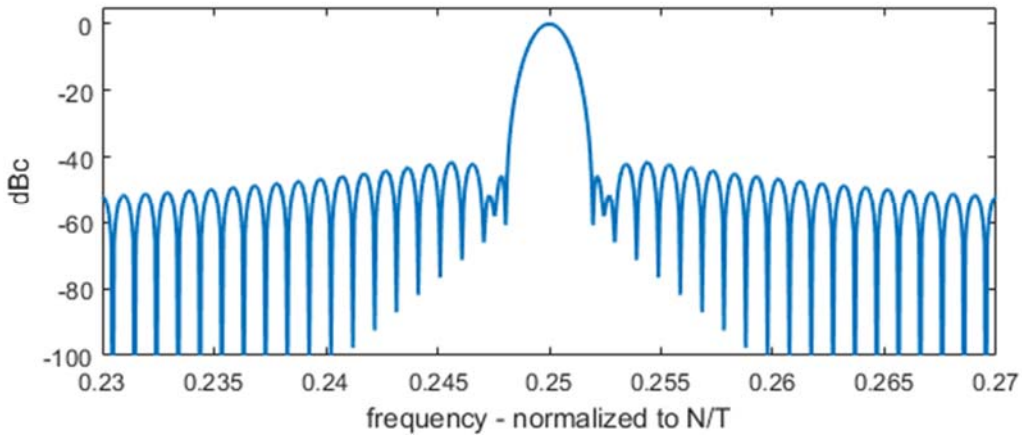

Figure 30. Zoomed rendering of Figure 29.

4.8 Discussion

One might ask whether uniformly sampled data can be resampled to nonuniform spacing and processed accordingly to advantage. Regrettably, this is not viable to remedy aliasing or Doppler ambiguity because the resampling process inherently assumes antialiasing filters built into the interpolation filter.[30] Consequently, since the aliasing is already "built in" to the data, it is not affected by subsequent processing, including interpolation.

While several deterministic sample-spacing functions have been presented here, it takes little imagination to construct other functions, some which might offer specific attributes desirable for some particular application. Important parameters for radar applications will be that $g'(z)$ and $g(z)$ conform to the characteristics discussed in section 3.3, with perhaps the additional constraint that $g'(z)$ be always greater than some minimum value determined by range-ambiguity requirements.

4.9 Spectrum Disambiguation

The real power of nonuniform sampling may be exemplified by examining the case of a signal with multiple frequencies. Accordingly, we put forth an example with the sum of three equal-amplitude tones with the following frequencies.

frequency #1 = $0.25\,N/T$,
frequency #2 = $-0.8\,N/T$, and
frequency #3 = $1.6\,N/T$.

Figure 31 illustrates the spectrum using Hann weighting with uniform sample spacing. Note that characteristic aliasing renders problematic ambiguity of the spectrum.

Figure 32 illustrates the spectrum using Hann weighting but with log-periodic sample spacing as described in Figure 22. We note that what otherwise would have been aliased signals have been smeared to render essentially background noise, thereby clearly revealing the true disambiguated spectral components.

Figure 33 illustrates the same calculations as Figure 32, except that 16 times the number of signal data samples were used, but with constant ratio N/T , implying T was extended by the same factor. Note the background smearing is to a significantly lower level.

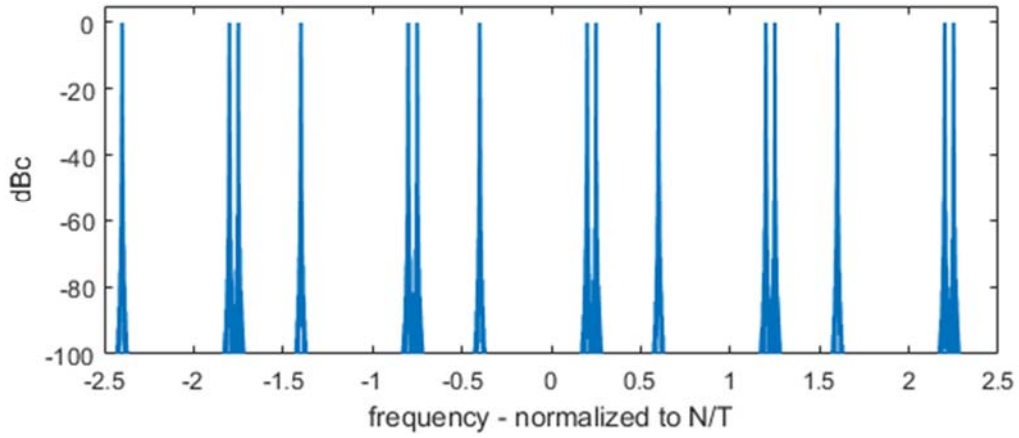

Figure 31. Spectrum of input signal using Hann window taper function, and uniform sample spacing.

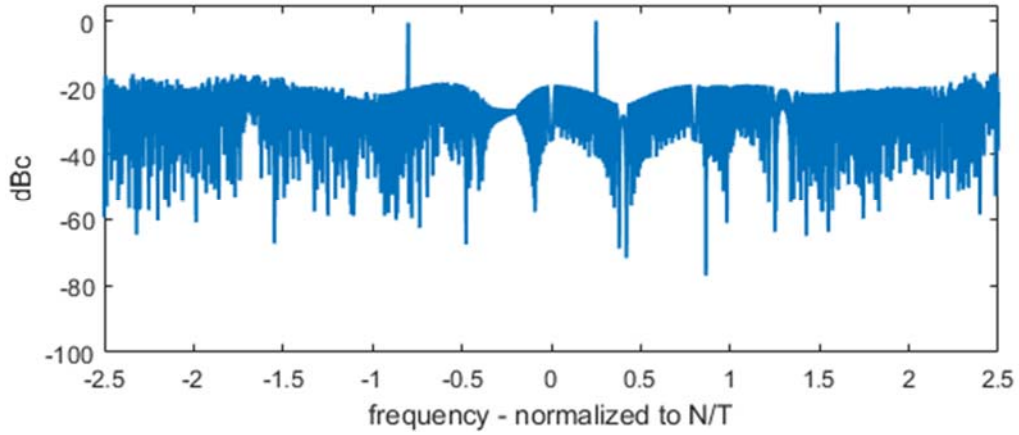

Figure 32. Spectrum of input signal using Hann window taper function, and log-periodic sample spacing.

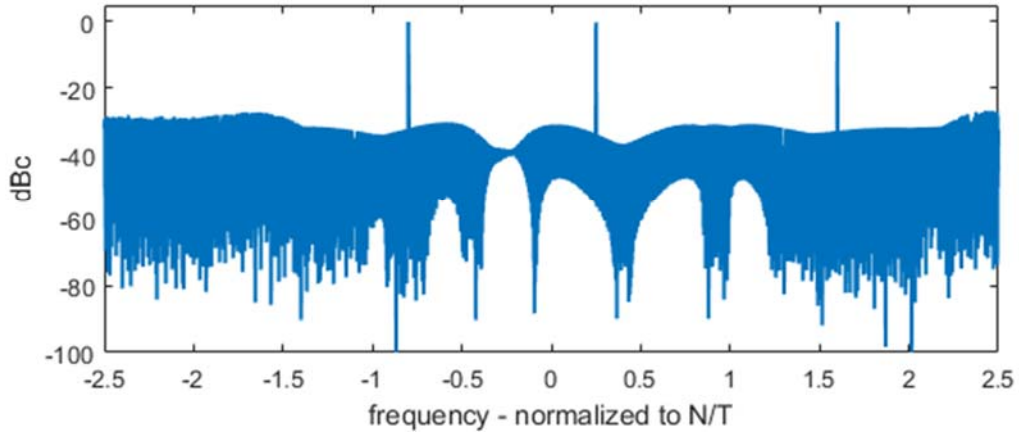

Figure 33. Same as Figure 32, except with 16 times the number of signal data samples.

"The New England Journal of Medicine reports that 9 out of 10 doctors agree that 1 out of 10 doctors is an idiot."
-- Jay Leno

5 Conclusions

We reiterate the following key points.

- Nonuniform (aperiodic) sampling allows disambiguation of radar Doppler, with attendant advantages in reducing grating lobes, blind velocities, and perhaps even improved SNR in the processed spectrum.

- Proper spectrum estimation requires nonuniform samples to be scaled in amplitude proportional to their instantaneous pulse sampling period. Optimal spectrum estimation also requires accounting for the actual sample times.

- Any window taper functions employed for sidelobe control require additional sample amplitude scaling according to the pulse position in the overall data collection interval.

- The nonuniform sample spacing can be specifically chosen such that any additional amplitude scaling to effect a window taper function is not required. This allows maximum SNR even with the benefits of improved sidelobe response equivalent to having employed a window taper function in the processing.

- Employing smooth variations in sample spacing often allows a cleaner spectrum. This suggests that a smooth deterministic sample-spacing modulation is preferable to one with random steps or jumps.

"Get your facts first, then you can distort them as you please."
-- Mark Twain

Appendix A – Weighted Sums and Noise

Here we examine weighting sums of noisy samples to minimize noise. This problem is one of essentially deriving an optimal filter, which can be found in numerous text books and articles. Here we present a very simplified version. We will use the method of Lagrange multipliers.

We will assume N data samples, each with identically distributed but independent zero-mean Additive White Gaussian Noise (AWGN).

Without loss of generality, we shall for the moment assume a DC signal of constant unit values for each sample.

We want to find an optimum linear weight vector, $\mathbf{w}$, applied to a noisy signal vector, $\mathbf{x}$. Optimality requires a choice, for which the standard choice is to minimize the Mean Squared Error (MSE). This optimization is typically performed subject to some constraint on the solution. Accordingly, we define several relevant parameters as follows.

$$\mathbf{x} = \begin{bmatrix} x_0 & x_1 & \ldots & x_{N-1} \end{bmatrix}^T = \text{noisy measurement vector, and}$$
$$\mathbf{w} = \begin{bmatrix} w_0 & w_1 & \ldots & w_{N-1} \end{bmatrix}^T = \text{weight vector which combines the measurements.} \tag{A1}$$

We identify the superscript '*' as the conjugate, the superscript 'T' as the transpose, and the superscript 'H' as the conjugate transpose. Both vectors are of length N.

In general, the noisy measurement vector is a signal corrupted by AWGN. That is

$$\mathbf{x} = \mathbf{s} + \mathbf{n}\,, \tag{A2}$$

where the constituent components are

$\mathbf{s}$ = signal vector, and
$\mathbf{n}$ = noise vector. (A3)

We define a constraint based on an input vector; a DC signal of unit value, namely

$$\mathbf{v}_d = \begin{bmatrix} 1 & 1 & \ldots & 1 \end{bmatrix}^T = \text{signal vector for the constraint.} \tag{A4}$$

We desire a weight vector that yields the proper result for the input signal vector of interest. To force a non-trivial solution, our constraint is then

$$\mathbf{w}^H \mathbf{v}_d = N\,. \tag{A5}$$

Basically, we want the sum of our weights to equal N. This means our DC gain is N.

To proceed, we identify the relevant second moment as

$$E\left\langle \left| \mathbf{w}^H \mathbf{x} \right|^2 \right\rangle = \mathbf{w}^H E\left\langle \mathbf{x}\mathbf{x}^H \right\rangle \mathbf{w} = \mathbf{w}^H \mathbf{R}_{\mathbf{xx}} \mathbf{w} \,, \tag{A6}$$

where

$$\begin{aligned} &E\langle y \rangle \text{ = is the expected value of } y \text{, and} \\ &\mathbf{R}_{\mathbf{xx}} = E\left\langle \mathbf{x}\, \mathbf{x}^H \right\rangle \text{ = the covariance matrix of } \mathbf{x}\,. \end{aligned} \tag{A7}$$

We may also readily calculate that $\mathbf{R}_{\mathbf{xx}}$ is the sum of constituent covariance matrices

$$\mathbf{R}_{\mathbf{xx}} = \mathbf{R}_{\mathbf{ss}} + \mathbf{R}_{\mathbf{nn}} \,, \tag{A8}$$

where

$$\begin{aligned} &\mathbf{R}_{\mathbf{ss}} = E\left\langle \mathbf{s}\, \mathbf{s}^H \right\rangle \text{ = the covariance matrix of } \mathbf{s}\text{, and} \\ &\mathbf{R}_{\mathbf{nn}} = E\left\langle \mathbf{n}\, \mathbf{n}^H \right\rangle \text{ = the covariance matrix of } \mathbf{n}. \end{aligned} \tag{A9}$$

Our minimum noise estimate occurs when $\left| \mathbf{w}^H \mathbf{n} \right|^2$ is minimized in the statistical sense. This means we wish to minimize

$$E\left\langle \left| \mathbf{w}^H \mathbf{n} \right|^2 \right\rangle = \mathbf{w}^H E\left\langle \mathbf{n}\mathbf{n}^H \right\rangle \mathbf{w} = \mathbf{w}^H \mathbf{R}_{\mathbf{nn}} \mathbf{w}\,. \tag{A10}$$

Using the method of Lagrange multipliers, we can construct the Lagrange function

$$\Lambda = \mathbf{w}^H \mathbf{R}_{\mathbf{nn}} \mathbf{w} + \lambda\left(\mathbf{w}^H \mathbf{v}_d - N \right) + \lambda^*\left(\mathbf{v}_d^H \mathbf{w} - N \right), \tag{A11}$$

where to maintain consistency with the literature, we identify for this development

$$\lambda \text{ = the Lagrange multiplier.} \tag{A12}$$

We may then find the optimum weight vector by taking the derivative of the Lagrange function with respect to $\mathbf{w}^H$ and setting it to zero. Doing so yields

$$\mathbf{R}_{\mathbf{nn}} \mathbf{w}_{opt} - \lambda \mathbf{v}_d = 0 \,, \tag{A13}$$

where we identify the specific solution

$$\mathbf{w}_{opt} = \text{the optimum weight vector } \mathbf{w}\,, \tag{A14}$$

which may be further rearranged to solve for

$$\mathbf{w}_{opt} = \lambda \mathbf{R}_{\mathbf{nn}}^{-1} \mathbf{v}_d\,. \tag{A15}$$

Plugging into the earlier constraint equation Eq. (A5) yields

$$N = \mathbf{w}_{opt}^H \mathbf{v}_d = \lambda^* \mathbf{v}_d^H \mathbf{R}_{\mathbf{nn}}^{-1} \mathbf{v}_d\,. \tag{A16}$$

We may then solve this scalar equation for the Lagrange multiplier as

$$\lambda^* = \lambda = N \left(\mathbf{v}_d^H \mathbf{R}_{\mathbf{nn}}^{-1} \mathbf{v}_d \right)^{-1}. \tag{A17}$$

We observe that λ is a real scalar (constant). Finally, combining Eq. (A17) with Eq. (A15), we arrive at the result for the optimum weight vector as

$$\mathbf{w}_{opt}^H = N \left(\mathbf{v}_d^H \mathbf{R}_{\mathbf{nn}}^{-1} \mathbf{v}_d \right)^{-1} \mathbf{v}_d^H \mathbf{R}_{\mathbf{nn}}^{-1} \tag{A18}$$

Note that we have made use of several identities from complex calculus and properties of the covariance matrix, including

$$\begin{aligned} &\frac{d\mathbf{w}}{d\mathbf{w}^H} \text{ is undefined,} \\ &\mathbf{R}_{\mathbf{nn}}^H = \mathbf{R}_{\mathbf{nn}}\text{, and} \\ &\left(\mathbf{R}_{\mathbf{nn}}^{-1} \right)^H = \mathbf{R}_{\mathbf{nn}}^{-1}\,. \end{aligned} \tag{A19}$$

For identically distributed but independent zero-mean AWGN, we may without loss of generality assume

$$\mathbf{R}_{\mathbf{nn}} = \mathbf{I} \text{ = identity matrix.} \tag{A20}$$

Therefrom we may calculate the optimum weights to be

$$\mathbf{w}_{opt}^H = N \left(\mathbf{v}_d^H \mathbf{R}_{\mathbf{nn}}^{-1} \mathbf{v}_d \right)^{-1} \mathbf{v}_d^H \mathbf{R}_{\mathbf{nn}}^{-1} = N \left(N \right)^{-1} \left[1 \quad 1 \quad \ldots \quad 1 \right], \tag{A21}$$

which we can simplify to

$$\mathbf{w}_{opt} = \left[1 \quad 1 \quad \ldots \quad 1 \right]^T. \tag{A22}$$

We summarize this result by stating that the optimum (in the squared-error sense) weighting of samples is a uniform amplitude weighting. This means that a uniform weighting will minimize the noise, and thereby maximize the Signal-to-Noise Ratio (SNR) of the sum. Obviously, departing from a uniform weighting will reduce the SNR of the sum from the maximum that would otherwise be achievable.

References

[1] Armin W. Doerry, *Basics of Polar-Format Algorithm for Processing Synthetic Aperture Radar Images*, Sandia National Laboratories Report SAND2012-3369, Unlimited Release, May 2012.

[2] Armin W. Doerry, Edward E. Bishop, John A. Miller, *Basics of Backprojection Algorithm for Processing Synthetic Aperture Radar Images*, Sandia National Laboratories Report SAND2016-1682, Unlimited Release, February 2016.

[3] Armin Doerry, *GMTI Processing using Back Projection*, Sandia National Laboratories Report SAND2013-5111, Unlimited Release, July 2013.

[4] Merrill I. Skolnik, *Introduction to Radar Systems – second edition*, ISBN 0-07-057909-1, McGraw-Hill, Inc., 1980.

[5] Merrill Skolnik (ed.), *Radar Handbook – third edition*, ISBN 978-0-07-148547-0, McGraw-Hill, Inc., 2008.

[6] Gaspare Galati, *Advanced Radar Techniques and Systems*, ISBN 0-86341-172-X, Peter Peregrinus Ltd., on behalf of Institute of Electrical Engineers, 1993.

[7] D. Curtis Schleher, *MTI and Pulsed Doppler Radar with Matlab – second edition*, ISBN-13: 978-1-59693-414-6, Artech House, Inc., 2010.

[8] L. Vergara-Dominguez, "Analysis of the digital MTI filter with random PRI," *IEE Proceedings-F*, Vol. 140, No. 2, pp. 129-137, April 1993.

[9] B. Xia, J. Xu, Y.-N. Peng, X.-G. Xia, J. Tang, "Doppler ambiguity resolving for SAR moving targets via linear migration correction," *Electronics Letters*, Vol. 47, No. 7, 31st March 2011.

[10] Shengqi Zhu, Guisheng Liao, "A New Unambiguous Radial Velocity Estimation Approach of Ground Moving Targets for SAR System," *Proceedings of the 2011 IEEE Radar Conference (RADAR)*, pp. 702-705, 2011.

[11] Shengqi Zhu, Guisheng Liao, "Estimating Ambiguity Number of Radial Velocity for Ground Moving Targets from a Single SAR Sensor," *Proceedings of the 2011 XXXth URSI General Assembly and Scientific Symposium*, pp. 1-4, 2011.

[12] Yan Huang, Guisheng Liao, Jingwei Xu, Jie Li, "GMTI and Parameter Estimation via Time-Doppler Chirp-Varying Approach for Single-Channel Airborne SAR System," *IEEE Transactions on Geoscience and Remote Sensing*, accepted for publication, 2017.

[13] Bernard D. Steinberg, *Principles of Aperture and Array System Design – Including Random and Adaptive Arrays*, ISBN 0-471-82102-0, John Wiley & Sons, Inc., 1976.

[14] Y. Kim, D. L. Jaggard, "The Fractal Random Array," *Proceedings of the IEEE*, Vol. 74, No. 9, pp. 1278-1280, September 1986.

[15] Petri Jarske, Tapio Saramäki, Sanjit K. Mitra, Yrjö Neuvo, "On Properties and Design of Nonuniformly Spaced Linear Arrays," *IEEE Transactions on Acoustics, Speech, and Signal Processing*, Vol. 36, No. 3, pp. 372-380, March 1988.

[16] B. P. Kumar, G. R. Branner, "Generalized Analytical Technique for the Synthesis of Unequally Spaced Arrays With Linear, Planar, Cylindrical or Spherical Geometry," *IEEE Transactions on Antennas and Propagation*, Vol. 53, No. 2, pp. 621-634, February 2005.

[17] Y. T. Lo, "A Mathematical Theory of Antenna Arrays with Randomly Spaced Elements," *IEEE Transactions on Antennas and Propagation*, Vol. 12, No. 3, pp. 257-268, May 1964.

[18] Y. T. Lo, S. W. Lee, "A Study of Space-Tapered Arrays," *IEEE Transactions on Antennas and Propagation*, Vol. 14, No. 1, pp. 22-30, January 1966.

[19] Bernard D. Steinberg, "Comparison Between the Peak Sidelobe of the Random Array and Algorithmically Designed Aperiodic Arrays," *IEEE Transactions on Antennas and Propagation*, Vol. 21, No. 3, pp. 366-370, May 1973.

[20] H. Unz, "Linear Arrays with Arbitrarily Distributed Elements," *IRE Transactions on Antennas and Propagation*, Vol. 8, No. 2, pp. 222-223 , March 1960.

[21] Farokh Marvasti (ed.), *Nonuniform Sampling: Theory and Practice (Information Technology: Transmission, Processing and Storage)*, ISBN 0306464454, Springer, 2001.

[22] J. L. Yen, "On Nonuniform Sampling of Bandwidth-Limited Signals," *IRE Transactions on Circuit Theory*, pp. 251-257, December 1956.

[23] Michael S. Davis, Aaron D. Lanterman, "Aliasing in Recurrently Sampled Signals With an Application to Synthetic Aperture Imaging," *IEEE Transactions on Signal Processing*, Vol. 63, No. 12, pp. 3088-3095, June 15, 2015

[24] Akram Aldroubi, Karlheinz Gröchenig, "Nonuniform Sampling and Reconstruction in Shift-Invariant Spaces," *SIAM Review*, Vol. 43, No. 4, pp. 585–620, 2001.

[25] Jonathan A. Legg, Alan G. Bolton, Douglas A. Gray, "SAR moving target detection using non-uniform PRI," *Proceedings of EUSAR'96*, pp. 423-426, Königswinter, Germany, 1996.

[26] Armin W. Doerry, *Computed Tomography – the details*, Sandia National Laboratories report SAND2007-4252, Unlimited Release, July 2007.

[27] A. Requicha, "The Zeros of Entire Functions: Theory and Engineering Applications," *Proc. IEEE*, Vol. 68, No. 3, pp. 308-328, 1980.

[28] Armin W. Doerry, *Catalog of Window Taper Functions for Sidelobe Control*, Sandia National Laboratories report SAND2017-4042, Unlimited Release, April 2017.

[29] Armin W. Doerry, *Generating Nonlinear FM Chirp Waveforms for Radar*, Sandia National Laboratories report SAND2006-5856, Unlimited Release, September 2006.

[30] A. W. Doerry, E. Bishop, J. Miller, V. Horndt, D. Small, "Designing interpolation kernels for SAR data resampling," SPIE 2012 Defense, Security & Sensing Symposium, Radar Sensor Technology XVI, Vol. 8361, Baltimore MD, 23-27 April 2012.

"Either write something worth reading or do something worth writing."
-- Benjamin Franklin

Distribution

Unlimited Release

1	MS 0519	M. R. Lewis	5349	
1	MS 0519	A. W. Doerry	5349	
1	MS 0519	L. Klein	5349	
1	MS 0532	S. P. Castillo	5340	
1	MS 0899	Technical Library	9536	(electronic copy)

Sandia National Laboratories